

Design, development and ground testing of hingeless elevons for MAV using piezoelectric composite actuators

D. Dwarakanathan, R. Ramkumar, S. Raja* and P. Siva Subba Rao

Dynamics and Adaptive Structures, Structural Technologies Division, CSIR-National Aerospace Laboratories, Bangalore, India

(Received July 23, 2014, Revised December 3, 2014, Accepted December 8, 2014)

Abstract. A design methodology is presented to develop the hingeless control surfaces for MAV using adhesively bonded Macro Fiber Composite (MFC) actuators. These actuators have got the capability to deflect the trailing edge surfaces of the wing to attain the required maneuverability, besides achieving the set aerodynamic trim condition. A scheme involving design, analysis, fabrication and testing procedure has been adopted to realize the trailing edge morphing mechanism. The stiffness distribution of the composite MAV wing is tailored such that the induced deflection by piezoelectric actuation is approximately optimized. Through ground testing, the proposed concept has been demonstrated on a typical MAV structure. Electro-mechanical analysis is performed to evaluate the actuator performance and subsequently aeroelastic and 2D CFD analyses are carried out to see the functional requirements of wing trailing edge surfaces to behave as elevons. Efforts have been made to obtain the performance comparison of conventional control surfaces (elevons) with morphing wing trailing edge surfaces. A significant improvement in lift to drag ratio is noticed with morphed wing configuration in comparison to conventional wing. Further, it has been shown that the morphed wing trailing edge surfaces can be deployed as elevons for aerodynamic trim applications.

Keywords: micro air vehicle (MAV); macro fiber composite (MFC); morphing; aeroelasticity; computational fluid dynamics (CFD)

1. Introduction

Nature has always paved the way for the new developments in Science and technologies. Especially in the field of aeronautics, different bird's flight is simulated by many researchers in the past. Structural morphing i.e., imitating bird's wing action, is basically a shape changing exercise, where the elastic deformation of the wing will provide the required aerodynamic configurations to improve the maneuverability, flight performance and endurance of flying vehicles.

Various design methodologies and fabrication technologies are developed to address aerodynamic and structures related issues for the fixed wing aircraft in the past and tiny MAV's in recent years. Several passive and active morphing concepts have been demonstrated through ground experiments and wind tunnel testings on scaled or actual vehicles. In particular morphing actions like camber change, wing twist, span change and winglet are shown on airfoils and wings.

*Corresponding author, Ph.D., E-mail: raja@nal.res.in

Active morphing concept is developed using smart materials, namely Shape Memory Alloy (SMA), Piezoelectric, Shape Memory Polymer (SMP), Electro Active Polymer (EAP) etc., where these materials are employed either as mechanism or surface bonded on to the host structure as actuators. In contrast, the passive morphing is demonstrated through compliance mechanism, servomechanisms etc. Usually in wing morphing, the primary control surfaces are not morphed; rather the secondary control surface or unconventional structural deformation (leading edge/trailing edge of the wing) is made to enhance the aerodynamic performance. There are many challenges one has to solve, while developing a morphing wing technique; some of them are i) finding optimal wing geometry (low AR or high AR), ii) suitable airfoil section, iii) flexible structural materials, iv) actuating elements, v) miniaturized electronics and vi) affordable power sources etc.

In the low Reynolds number regime, Pelletier and Mueller (2000) have observed the absence of hysteresis (rapid decrease in C_l) on a thin cambered plate, representing a low aspect ratio wing. Therefore, it is feasible that a thin cambered MAV wing can be a suitable candidate to demonstrate an electromechanically actuated morphing wing technique (Black Kite MAV: BK MAV, Roshan *et al.*, 2011).

There are many researchers worldwide studied about the morphing mechanisms/structures for aircraft. Weisshaar (2013) has made an extensive review on the morphing techniques, regarding high-speed aircraft. Similarly Barbarino *et al.* (2011) have examined the merits and demerits of morphing technologies for aircraft, considering the weight budget, shape change and readiness level. Gomez and Garcia (2011) have assessed the potential application of morphing wing technology in unmanned aerial vehicles (UAV). However, it is understood that a compromise needs to be made towards vehicle performance, weight budget and power to fly a morphing wing. Sofla *et al.* (2010) have explored the application of smart materials in wing morphing; weight penalty has been found as a critical issue, while incorporating morphing technology in aircraft. Thus, future challenges toward the development of morphing wing using smart materials have to address better stiffness to weight and strength besides satisfying the required actuation authority. Kuder *et al.* (2013) have revisited the research approaches related to variable stiffness approach to a possible morphing wing solution for large version. Barbarino *et al.* (2014) have made an attempt to integrate the SMA (Shape Memory Alloys) on to the morphing wing. They have reported that when the SMAs are integrated within the multi-stable structure, then both power consumption and environmental issue like temperature variation can be better addressed.

The other noteworthy studies made by Kuder *et al.* (2013) and Barbarino *et al.* (2014) in this direction, have also addressed the use of SMA actuation in morphing applications where the power requirement is considered as a critical issue and also it is shown that integration of SMA wires onto wing structure poses definite challenge.

Modeling large thin membrane structures along with surface bonded piezoelectric composite actuator (MFC) is possible using the commercial software like ANSYS, ABAQUS in order to capture the electromechanical interaction through solid elements to characterize the piezoelectric behavior. Deraemaeker *et al.* (2009) have developed numerical unit cell model to compute the equivalent mechanical and piezoelectric properties of MFC in expansion and contraction mode and subsequently the properties validated with manufacturer supplied ones. To model MFC actuator, more number of solid elements are required due to aspect ratio criteria, which may demand the numerical model to be large by modifying the element size of the host structure in order to maintain the displacement continuity. Cote *et al.* (2004) have proposed a simple approach to model the piezoelectric behavior through thermal analogy for smart structures using MSC-NASTRAN.

Using this approach, Bradley and Peter 2012, Bradley and Peter 2013 have shown that MFC actuator can be modeled using shell element, which will eventually reduce the modeling time and degrees of freedom (dof). The thermoelastic constants are employed in this approach to represent the electromechanical coupling. Bilgen *et al.* (2007) have designed and demonstrated a morphing wing concept using unimorph MFC as elevon for a MAV (wingspan=0.76 m) in association with conventional elevator and rudder. An improved performance is noticed with reduced drag, increased bandwidth of the actuators and stable flights. Paradies and Ciresa (2009) have displayed roll moment control on a UAV wing using MFC actuators. Bilgen *et al.* (2010) have proposed an innovative solution for handling unbalanced (asymmetric) voltage of MFC actuators to operate in the range -500 V to 1500 V while morphing the structure. This has been achieved by using lightweight solid-state electrical circuit, employing conventional electrical components like diodes and resistors. Wickramasinghe *et al.* (2011) have developed a hybrid concept using MFC and Electro Active Polymer (EAP) for EA-MAV to achieve highly maneuverable condition, where MFC acts as the prime actuating system and EAP as ancillary one to amplify the deflection of conventional control surface. Troy *et al.* (2012) have tested MFC actuated airfoil in wind tunnel and observed that MFC actuated control surface in UAV has got sufficient control authority to provide a stable flight.

Bilgen *et al.* (2013) have demonstrated the morphing concepts on primary control surfaces (elevator, aileron, and rudder) using MFC actuators. In their approach, the existing conventional airfoil has been redesigned to adopt morphing capabilities in mini UAV. The successful flight trails have further shown that there is sufficient damage tolerance available with morphing control surface, when compared to conventional one. Pankonien and Inman (2013) have aerodynamically characterized spanwise morphing wing concept, showing that uniform morphing can be achieved under the influence of aerodynamic loads. Bilgen and Friswell (2014) have recently tested the concept of surface induced deformation of variable camber morphing wing using MFC actuators in wind tunnel. Under morphed condition, the wing has withstood the aerodynamic loads with a maximum free stream velocity of 22.8 m/s.

Ohanian *et al.* (2012) have studied the reliability of MFC actuators by operating them upto 1 million cycles on a mini UAV and discussed the advantages of using MFC over conventional servo actuators. Osgar *et al.* (2013) have brought out an overall comparison between conventional and piezoelectrically morphed control surface during flight testing of mini UAV. In general, MFC actuators have shown good potential with lesser mechanical loss, when compared to conventional servo actuators (due to linkages). LaCroix and Ifju (2012) have examined that MAV can be controlled by MFC actuators even though deformations produced by these actuators are small when compared to servo actuators.

Researchers have studied the importance of aeroelasticity/aerodynamics of mini UAVs with morphing wings (Sanders *et al.* 2003, Vale *et al.* 2011). They have observed increased roll rate, improvement in stall speed, endurance etc with conformable wing configurations. It is therefore understood that a conformable wing through morphing process provides a better aerodynamic performance and MFC actuators can be employed to achieve the trim conditions.

In the present paper, a study is made to achieve an optimal aerodynamic trimming condition using trailing edge morphing, induced by MFC actuation. BK MAV is a 300 mm span, inverse Zimmerman configured flying vehicle, which has got conventional control surfaces to achieve its aerodynamic trim conditions. For this flying MAV, we have designed a morphing wing with adaptive stiffness involving elastic stiffness and induced piezoelectric stiffness that are tailored through design analysis procedure using high fidelity FEA and CFD tools. The MFC actuators are

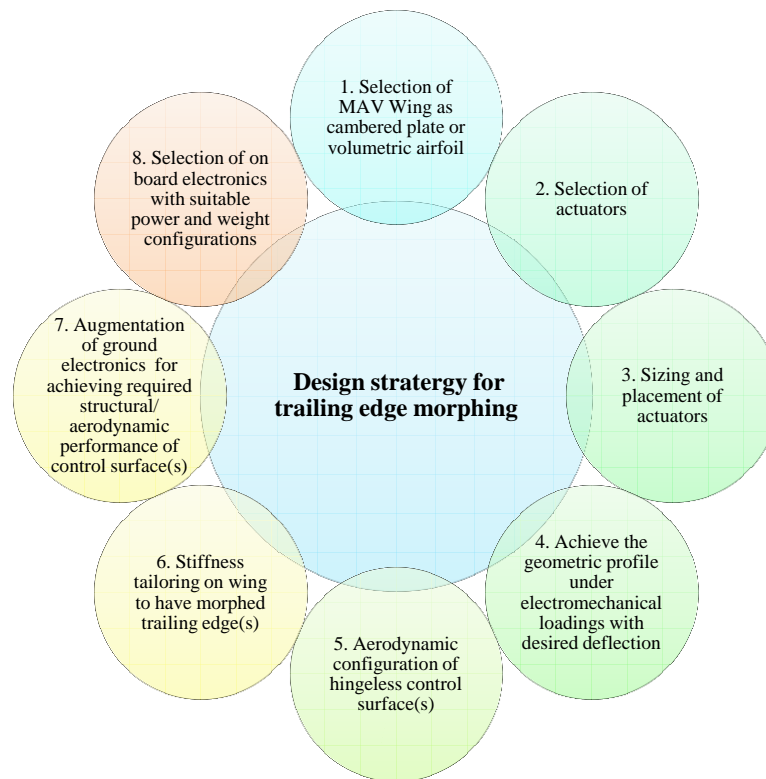


Fig. 1 Design methodology for the development of hingeless control surface using MFC actuators

successfully employed on morphing wing with ultra-lightweight in-flight electronics such as DC-DC convertors, amplifier circuits etc. These actuators are very flexible, thin in nature and develop the required actuation authority to elastically deform the wing trailing edge surface on which they are surface bonded.

2. Design methodology for morphing wing

Analytical and experimental studies are conducted on the MFC actuated structures, which have shown very promising results for MFCs to be considered in morphing wing applications. The structural couplings, namely the strains due to extension/compression are directly interacting with MFC actuation through an adhesive bonding layer. Therefore, integration of these tiny sized actuators on the structure becomes easier. The design and development procedure for fixed wing MAV with hingeless control surface concept is shown in Fig. 1.

2.1 Selection of MAV wing for morphing

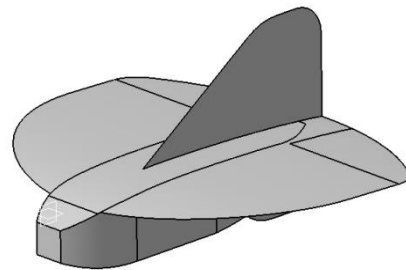
MAV airframe may be designed either as volumetric airfoil or as thin cambered plate (membrane structure). Pelletier and Muller (2000) have observed that cambered plate airfoil produces better aerodynamic characteristics than the thick airfoils. Also, the membrane structure

Table 1 BK MAV details

Parameters	Details
Weight	292 gms
Operational altitude	100 m AGL
Range	2 km radius
Endurance	30 min
Fuselage length	250 mm
Wing Span	300 mm
Root chord	250 mm
Aspect ratio	1.45
Planform area	0.064396 m ²
Mean aerodynamic chord	213 mm



(a) Cambered plate cross section



(b) CAD Model

Fig. 2 BK MAV details

of BK MAV is found to be good for morphing wing studies. The details of BK MAV are given in Table 1. The mean camber line of Selig 4083 airfoil has been considered with positive/negative thickness to form a cambered plate. The cross section of the plate wing is shown in Fig. 2, which has a t/c ratio of 0.32%.

2.2 Selection of actuators

There are different smart materials available commercially as actuators, namely Shape Memory Alloy (SMA), Shape Memory Polymer (SMP), Electro Active Polymer (EAP) and Piezoelectric actuator etc (Gomez and Garcia 2011, Sofla *et al.* 2010, Kuder *et al.* 2013). The actuator selection for morphing application are made based on the following requirements,

- i. Availability of miniaturized electronics to actuate the actuators,
- ii. Type of integration (Surface bonding or using mechanism),
- iii. Weight consideration.

Among the available smart materials, piezoelectric actuator (MFC) meets the design requirements for BK MAV. MFC actuator is a capacitive device and behaves as multifunctional; meaning it provides elastic stiffness once surface bonded on to the host plate besides acting as actuator and sensor. MFC can be operated in the voltage range of -500 V to 1500 V, which makes it very efficient under electromechanical coupling. Since it is environmentally protected and very

flexible, therefore provides an improved damage tolerance.

2.3 Sizing and placement of the actuator

According to the orientation of the piezoelectric fibers in the polymeric matrix system, MFC actuators (d_{33} / d_{31} type) may induce directional actuation both in expansion or contraction mode. MFC actuator is characterized with active width and length, which are considered for block force/free deflection calculation. The sizing is done to meet the following requirements,

- i. Maximum trailing surface deformation
- ii. Smooth contour of deflection (camber variation)
- iii. Size should be accommodated within the allotted wing area

Three MFC configurations (d_{33} type) are taken for the study, namely M4010, M8528 and M8557. The specifications of the actuators can be referred to Smart Materials Corp. ®, Germany. Numerical models for these MFCs are developed and are integrated with the FE model of BK MAV to examine their performances.

3. Piezoelectric-thermal analogy

The numerical model of the MFC has been built by comparing the piezoelectric and thermo-elastic strains respectively. A four noded shell element is used for this purpose and the electrical inputs are then converted into equivalent temperature loads, which are applied on the nodes of the FE model of MFC actuator (refer to Fig. 3).

Generally, the thermo-elastic constitutive equation can be expressed by the generalized Hooke's law in the form

$$\{\sigma\} = [C^E]\{\varepsilon\} - [C^E]\{\alpha\}\Delta T \quad (1)$$

Where, $\Delta T = T - T_0$, α is the thermoelastic coefficient.

By comparing the piezoelectric and thermo-elastic constitutive equations (Cote *et al.* 2004), we have

$$[d]^T \{E\} = \{\alpha\} \Delta T \quad (2)$$

Where d is the piezoelectric strain constant, E is the applied electric field.

Therefore, desired changes in voltage for the piezoelectric elements can be directly given as input into the FEM code via thermal analogy as changes in temperature of identical magnitude and also by using the actual piezoelectric properties (strain coupling terms). The coefficient of thermal expansion in low (<500V) and high electric field (>500V) and finger electrode width can be calculated using the following reduced relation

$$\alpha_1 = \frac{d_{11}}{h_a}; \alpha_2 = \frac{d_{12}}{h_a}; h_a = \frac{d_{11} \times V_{\max}}{\text{Free Strain}} \quad (3)$$

3.1 Numerical validation for MFC modeling

A single MFC actuator (7 layers) is idealized as an equivalent orthotropic lamina (Equivalent Single Layer) without a substrate, considering only its active area. The temperature load of 2000°C

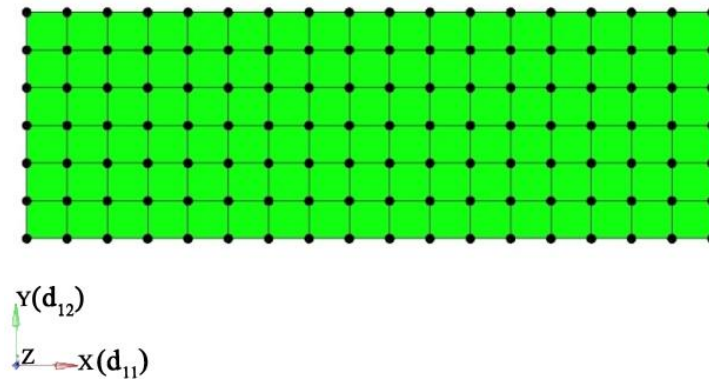


Fig. 3 Numerical model of MFC

Table 2 Mechanical properties of materials used in the analysis

Properties		MFC	GFRP Bi-Directional	Aluminium
Density (Kg/m ³)	ρ	5440	2000	2800
	E_1	30.336	13	70
Young's Modulus (GPa)	E_2	15.857	13	-
	E_3	15.857	-	-
	ν_{12}	0.31	0.2	0.3
Poisson's Ratio	ν_{23}	0.31	-	-
	ν_{13}	0.31	-	-
	G_{12}	5.515	4.4	-
Shear modulus (GPa)	G_{23}	5.515	4.4	-
	G_{13}	5.515	4.4	-
	Piezoelectric Strain Constant (High-Field/ Low-Field) (pm/V)	d_{11} (or d_{33})	460/ 400	-
d_{12} (or d_{31})		-210/-170	-	-

Table 3 MFC validation results

Model	Free Strain (μ)		Blocking force (N)	
	Manufacturer's Details	Thermal Analogy	Manufacturer's Details	Thermal Analogy
M4010	1400	1400	126	127
M8528	1800	1800	454	457
M8557	1800	1800	923	929

(Potential difference $\sim 2000V$; -500 to 1500 V) is applied on each node, keeping the reference temperature (T_0) as $0^\circ C$.

The parameters like free strain and block force of the MFC actuator are obtained through analysis by thermal analogy and they are compared with available data in the open source (Smart Material Corp.®). The material data presented in Table 2 is used in the analysis. In Table 3, the results are given; where one can see a good agreement between numerical analysis and the data from manufacturer.

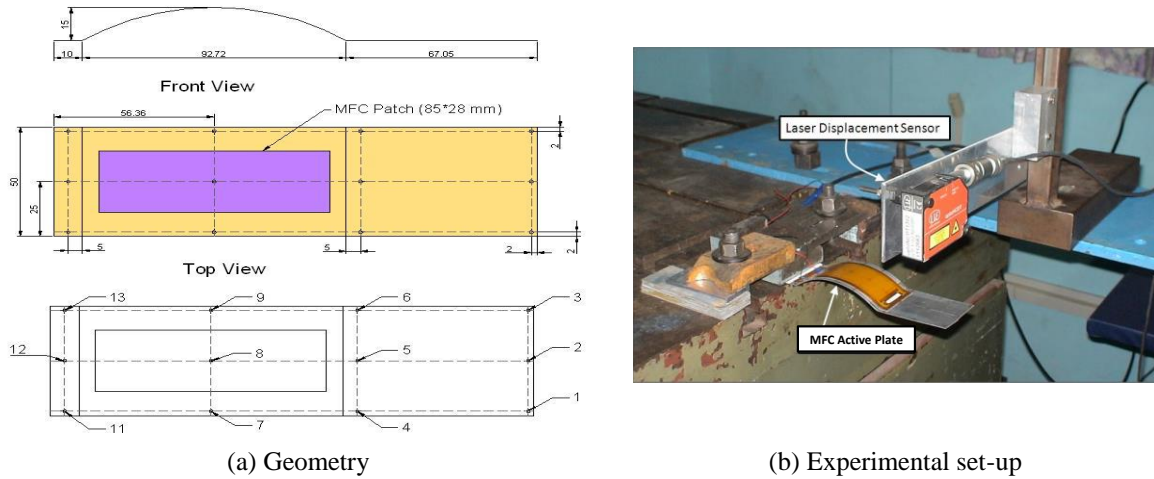


Fig. 4 MFC modelling validation with experiments

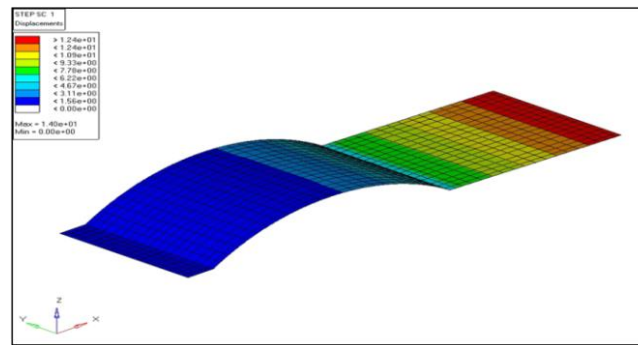


Fig. 5 Deflection contour of curved plate with MFC at 1500 V

3.1.1 Induced strain validation

Having validated the MFC patches independently in fully constrained (for block force) and an unconstrained (for free deflection) state, the next stage of analysis is carried out to characterize them on an elastic substrate. This is very important task as these MFC patches need to be adhesively bonded on to the substrate, where their locations/ sizes play a vital role in deciding the induced force/ deflection.

For this purpose an aluminum (AL) curved plate with a dimension of $170 \times 50 \times 0.4 \text{ mm}^3$ has been taken and a MFC 8528 patch is surface bonded on this plate (refer to Fig. 4). An experimental set up is made for the clamped-free curved AL plate with surface bonded MFC actuator to conduct static piezoelectric testing. A laser displacement sensor unit is used to measure the plate tip deflection. Also, a numerical model is developed using shell element and analyzed for the tip deflection. The deflection results are shown in Fig. 5.

The transverse tip deflection of the AL plate is presented in Fig. 6 for various input voltages. The experimental and piezoelectric thermal analogy results are then compared. We have observed a close match between them, which has brought out the required confidence in the thermal analogy, adopted for morphing wing analysis in the applied voltage range -500 to 1500 V.

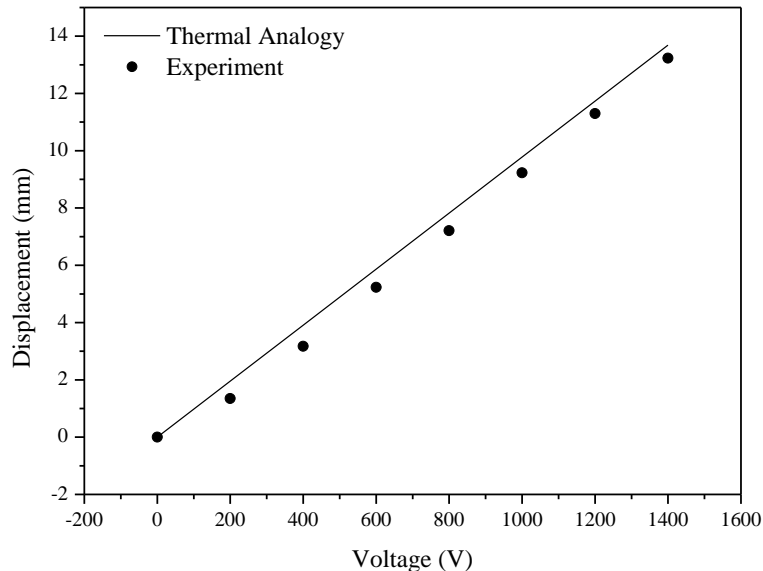


Fig. 6 Deflection Vs applied voltage for curved plate with MFC actuation

Table 4 MAV airframe details

Components	No. of Layers	Thick/Layer (mm)	Thickness (mm)	Orientation	Material
Wing	2	0.22 /0.22	0.45	0°/0°	GFRP
Elevon	1	0.16	0.16	0°	GFRP
Wing Stiffener	3	0.22/0.22/0.22	0.66	0°/0°/0°	GFRP
Fuselage	4	0.25/0.25/0.25/0.25	1	0°/90°/0°/90°	GFRP

4. Development of hingeless control surface for MAV

BK MAV is a thin cambered plate, made up of bi-directional glass fabric (GFRP) materials. Before addressing the MFC placement and its sizing, the conventional wing of BK MAV has been optimized for its stiffness distribution to accommodate MFC in order to produce the required deflection, satisfying the following conditions:

- i. To withstand the aerodynamic loads,
- ii. Provide the needed flexibility for the wing to be morphed.

The complete structural details are presented in Table 4.

Two MFC actuators are surface bonded, one on the starboard and the other on the port side of the wing. Using thermal analogy approach, analysis is carried out and the results are presented in Table 5. Here we have observed that M8557 gives maximum deflection but the weight of the actuator is more than M4010, which induces relatively less deflection. However, M8528 provides optimally the necessary deflection with an acceptable weight penalty and hence it is selected for morphing study.

In order to achieve a desired deflected profile of elevons using MFC actuators, they have to be placed in spanwise direction to produce a continuous camber change of the wing trailing edge surface. Therefore, optimal spanwise and chordwise locations for these actuators have to be

Table 5 Actuator selection

MFC	Displacement (mm) @ 1500 V	Weight (gms)
4010	4.86	0.6528
8528	7.80	3.88
8557	7.93	7.9

Table 6 Actuator location sizing

MFC	Spanwise location (% b/2)	Displacement (1500V) (mm)
	25	7.87
8528	35	7.73
	50	6.59

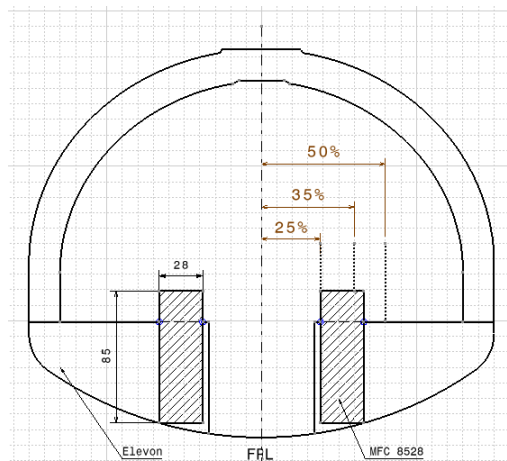


Fig. 7 Different spanwise position of MFC

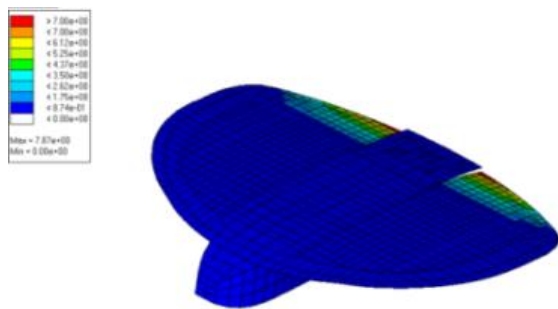


Fig. 8(a) Numerical simulation at 1500V

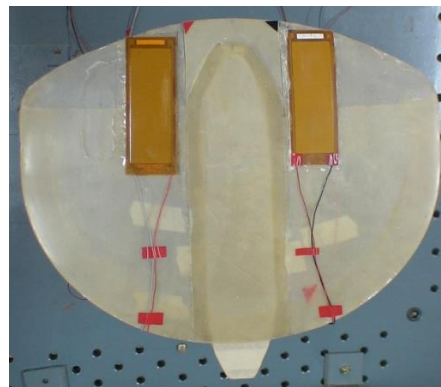


Fig. 8(b) Fabricated MAV

identified for maximum trailing surface deformation. It is understood that chordwise MFC location is very critical to achieve maximum deflection. Initially three spanwise locations are considered, namely 25%, 35% and 50% of wing semi span from fuselage reference line (FRL), which is

schematically shown in Fig. 7. The achieved trailing wing surface displacement with respect to different location of MFC actuator is given in Table 6. It is evident that the location of 25% gives maximum deformation, thus this actuator location is finalized for morphing study.

In the trailing surface morphing, the wing is elastically deformed under the MFC actuation force, which is developed in between the actuator layer and GFRP structure (host) under the applied electric voltage. The FE model of BK MAV and the deflection contour at 1500V is shown in Fig. 8(a). Subsequently, the MAV structure is fabricated and two MFC actuators are surface bonded on the wing. The fabricated MAV can be seen in Fig. 8(b).

5. Experimental study on morphing winged MAV

BK MAV is basically a hand launched vehicle and it is operated by remote control. Therefore, to operate the MFC actuator during in-flight, they have to be actuated by remote control. To facilitate the above requirement, we have employed the miniaturized electronics for ground studies.

AMD2012-CE3 High Voltage Amplifier is used as a DC-DC converter to drive the MFC patch. According to the voltage input (polarity), the MFC patch on MAV either elongates or contracts. The control surface deflection of MAV, actuated by MFC is measured using a laser displacement sensor unit. LIPO battery is used to power up the RF receiver and high voltage amplifier. Based on the input signal from transmitter, the DC-DC converter generates -500 to 1500 V to actuate MFC patch on the MAV wing. The block diagram used for ground test is shown in Fig. 9. In Table 7, a comparison is made between electronics and their weights of the conventional servomechanism to MFC actuators.

Under the MFC actuation, there is a continuous camber change observed in the trailing wing surface of MAV. When negative voltage is applied, the wing trailing surface is morphed upward and at positive voltage, it is morphed downward. The deflection contour is noticed 65 mm from the wing trailing edge effectively, in contrast to the 44 mm chord of conventional elevon in BK MAV. This indeed has increased effective area of morphed trailing surface over the conventional elevon. Therefore, it is realized that the deformed surfaces can be employed as elevator and aileron for achieving the required trim conditions. The upward and downward camber changes are shown

Table 7 Comparison of electronics weight budget for the morphing with conventional control surface

Sl. No	MFC based control surface electronics	Per unit (in gms)	Conventional control surface electronics	Per unit (in gms)
1	High voltage DC-DC amplifier (AMD2012-CE3A)	14.0	Servo with wire	9.0
2	Wiring for DC-DC amplifier to connect to ESC (Electronic Speed Controller)	3.0	Link rod	3.0
3	1 MFC (85×28)	3.7	Control horn	2.0
4	Adhesive for MFC	1.0	Linkage stopper and bolts	3.0
5	Wiring for MFC to connect to DC-DC amplifier	1.0		-
	Total Weight in grams	22.7		17.0

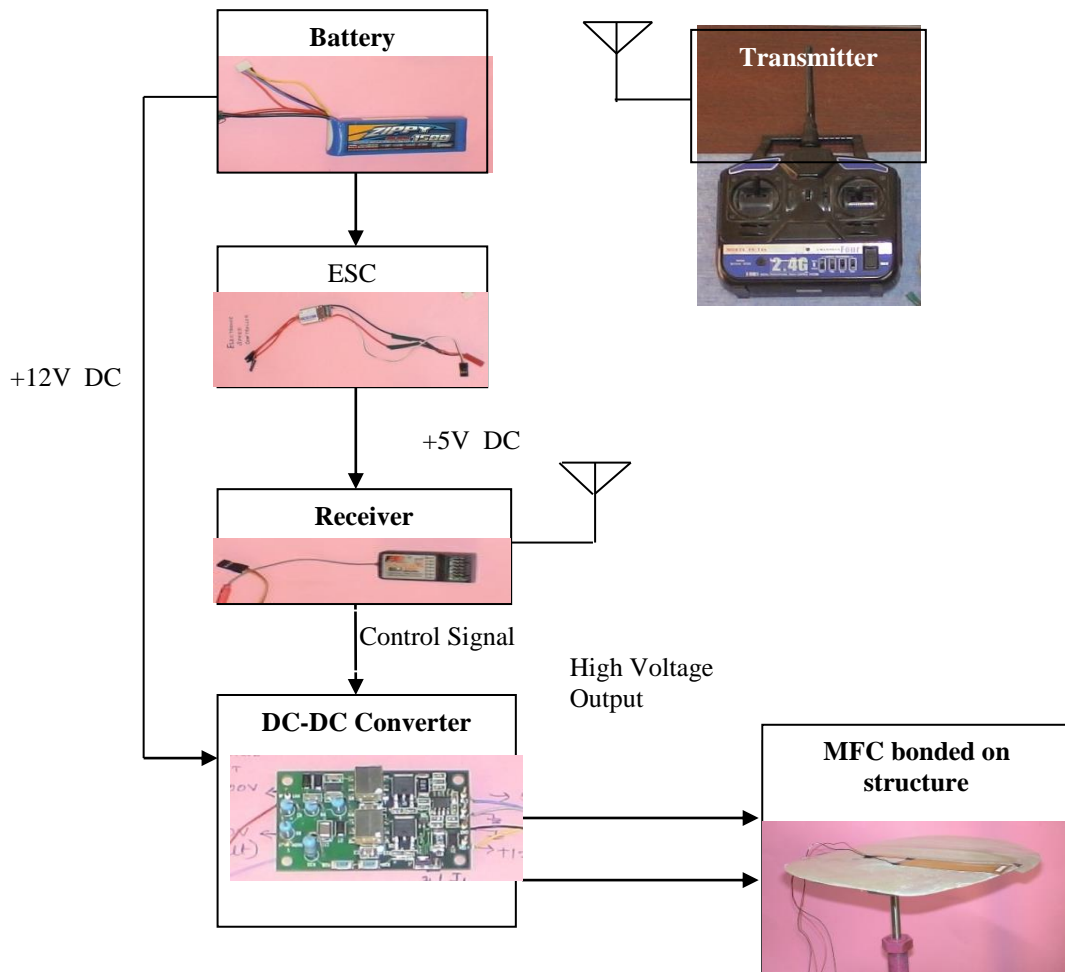


Fig. 9 Block diagram

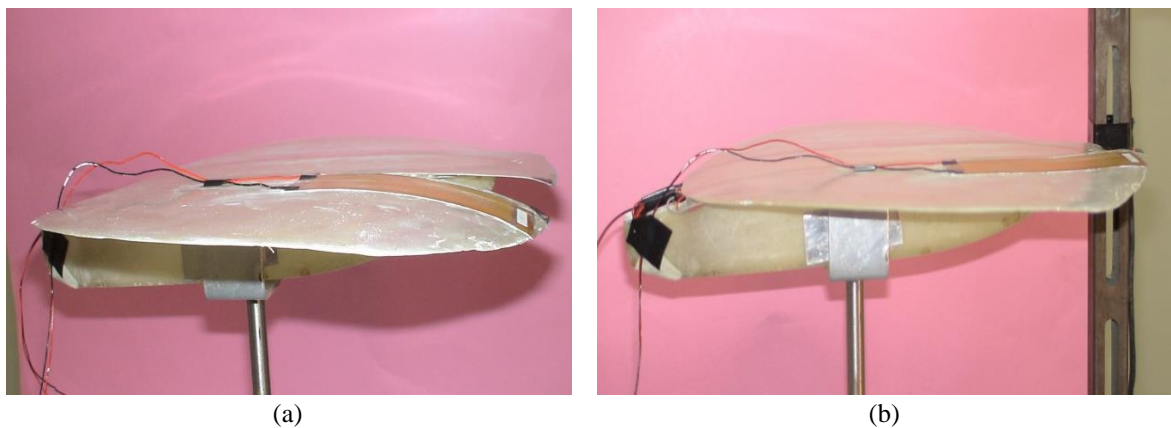


Fig. 10 (a) Downward camber change (b) Upward camber change

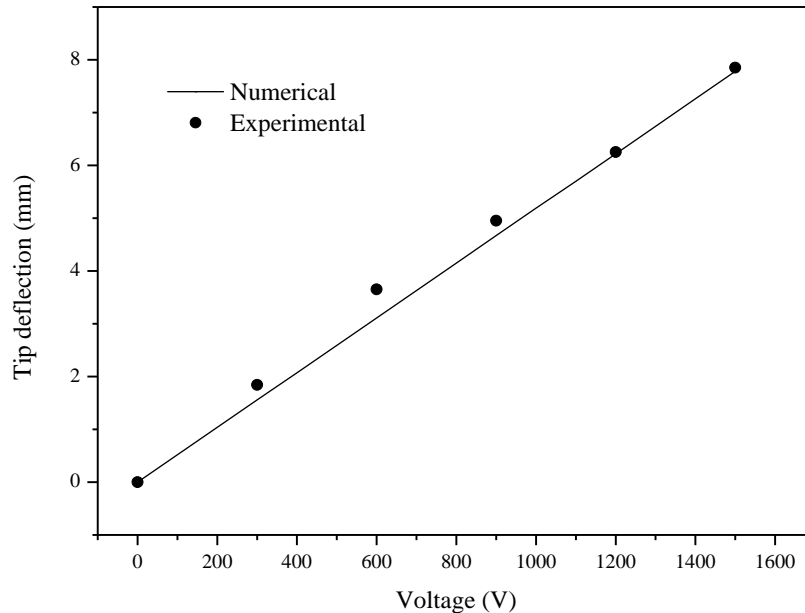


Fig. 11 BK MAV trailing surface deformation

in Fig. 10. At 1500V, a maximum tip deflection of 7.8 mm and at -500V, a maximum tip deflection of -3 mm are observed. The deflections at different applied voltages are plotted in Fig. 11.

It can be seen that the numerical simulation using thermal analogy has closely predicted the tip deflections under MFC actuation at 300 V, 600 V, 900 V, and 1500 V, respectively. Using these two MFC actuators, the trailing surfaces of the MAV wing are deformed to the required amplitude and area. However, a careful examination is needed to assess the deformed wing part(s) to be considered as elevator or aileron in flight operation of MAV. We have adopted aeroelastic and CFD analysis tools to evaluate the aerodynamic performances of morphed wing trailing surface(s).

6. Aeroelastic analysis of morphed wing

The control surface performance of BK MAV is analyzed in terms of control derivatives. The control derivatives indeed measure the change in forces and moments, which has occurred due to the deflection of trailing edge morphing. Subsequently using these control derivatives, we can calculate the effectiveness of the control surface(s). In the present study, we have considered the morphed trailing wing surfaces, as elevons; so the performance is presented for elevator and aileron mode separately. The performance of morphed trailing surface and conventional elevon has been evaluated and the results are compared.

Fig. 12 (a), (b) shows the planform configurations of morphed and conventional wings with control surfaces. The structural model and aerodynamic model of the BK MAV are made to carry out the static aeroelastic analysis (see Fig. 13) in MSC NASTRAN. Table 8 shows the details of static aeroelastic analysis.

Table 9 Elevator mode derivatives of morphed and conventional control surfaces

Parameter	Conventional	Morphed	Improvement (%)
$C_{L\delta e}$	0.387/rad	0.485/rad	20
$C_{M\delta e}$	-0.15/rad	-0.165/rad	9

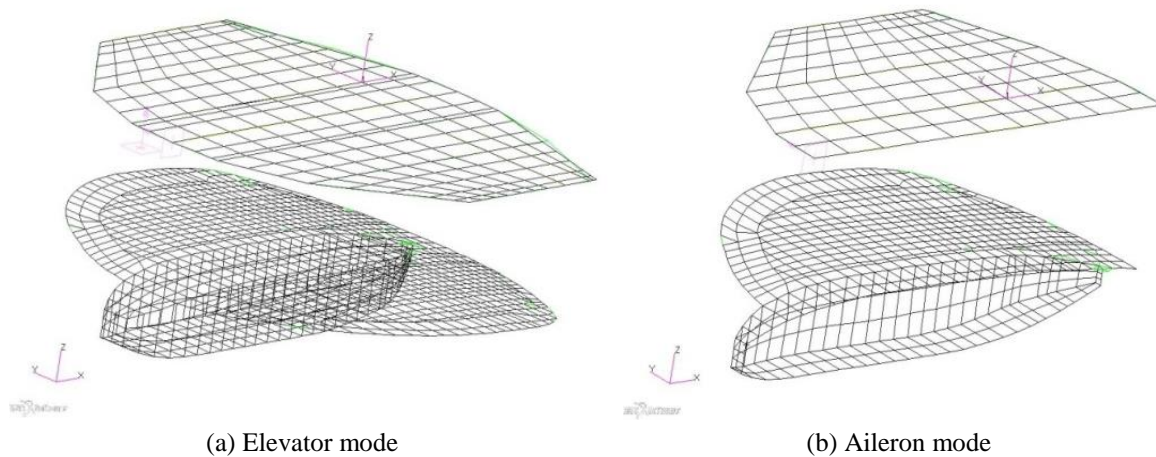


Fig. 13 FE Model used in aeroelastic analysis

Table 10 Aileron mode derivative of morphed and conventional control surfaces

Parameter	Conventional	Morphed	Improvement (%)
$C_{L\delta a}$	0.103/rad	0.144/rad	28

the aerodynamic performances of conventional and morphed control surfaces. A significant improvement is noticed with hingeless control surface (morphed) over the conventional ones.

6.2 Aileron mode

When the wing trailing edge surfaces are deflected anti-symmetrically by 3 mm with +500/-500 V applied to MFC actuators, around ± 2.65 deg angle of deflection is obtained. The static aeroelastic trim analysis, considering aileron mode is performed and the results for both conventional and morphed configurations are compared in table 10.

The wing flexibility in MAV may reduce the control surface effectiveness. In BK MAV, the elevon deflection produces a twisting moment, which will eventually reduce the incidence angle of MAV. Therefore, it is essential to estimate at what air speed, $C_{L\delta a}$ will change from positive to negative, in order to obtain the point of aileron reversal. The analysis on conventional and morphed configurations has shown very interesting results, which are presented in Fig. 14. The morphed wing torsional stiffness is good enough to produce better margin due to the additional stiffness contribution coming from induced strain/force (active stiffness). In the complete flight envelope, the piezoelectrically morphed wing has produced the best aileron performance (15 to 40 m/sec).

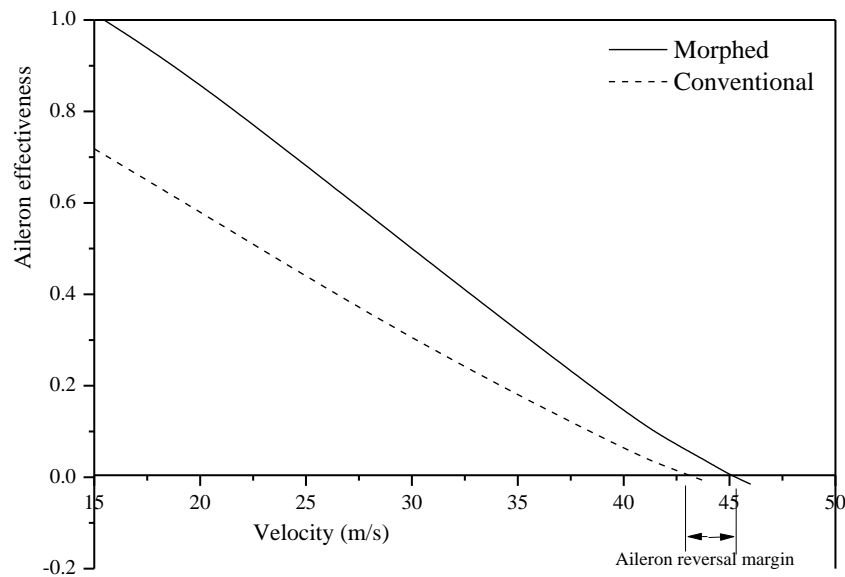


Fig. 14 Aileron reversal speed enhancement

Table 11 Roll performance of BK MAV

Parameter	Conventional	Morphed	Improvement (%)
Roll rate (deg /sec)	192.2	268.7	28
Bank angle (deg)	20.16	30.8	34
Radius of turn (m)	62.47	38.47	38
Turn rate (deg/sec)	13.75	22.0	38

6.3 Roll maneuver performance

BK MAV requires high maneuverability to meet its various surveillance applications. As such, the characteristics of control surfaces play a key role to achieve all these mission requirements. BK MAV will make a level banked turn maneuver, when morphed wing trailing surfaces deflected antisymmetrically. The roll maneuver is examined therefore in terms of roll rate (deg/sec), bank angle (deg), radius of turn (m) and turn rate (deg/sec), respectively. The control derivatives are then computed from static aeroelastic analysis using MSC NASTRAN on both conventional and morphed wings. With minimum turn radius and maximum turn rate, if the MAV can do the required roll maneuver then it is considered as good performance because the control surface is in deployed condition for less time. From Table 11, one can notice that a significant improvement is achieved by the morphed wing to produce better roll performance on BK MAV.

7. CFD simulation for morphed and conventional cambered plate

In the morphing process, we have achieved a smooth, continuous camber variation of contour along the trailing surface, which is different from the conventional servo actuated deflection

contour. Therefore, analysis is made to understand, how the aerodynamic flow parameters are changing between morphed and conventional contours of deflection through computational fluid dynamic simulation. The coefficients of lift and drag are computed to evaluate the aerodynamic efficiency. Since BK MAV is operated in the low Reynolds number regime, its effect on the aerodynamic characteristics is highly dependent on the surface finish and profile of the aerodynamic configuration. Ohanian *et al.* (2012) have shown that the conformal shape changes may result in efficient control force generation, higher lift, and superior lift-to-drag ratio etc. Nevertheless, they have demonstrated only on morphing airfoil section not for the cambered morphed plate as in the present study.

The ANSYS FLUENT CFD tool is used for simulation and Spalart-allmaras turbulent model with near wall function is employed. Standard sea level conditions are taken, with the flight velocity of 15 m/s and Reynolds number of approximately 2,47,000. There are two cases considered, namely upward and downward deflection of cambered plate.

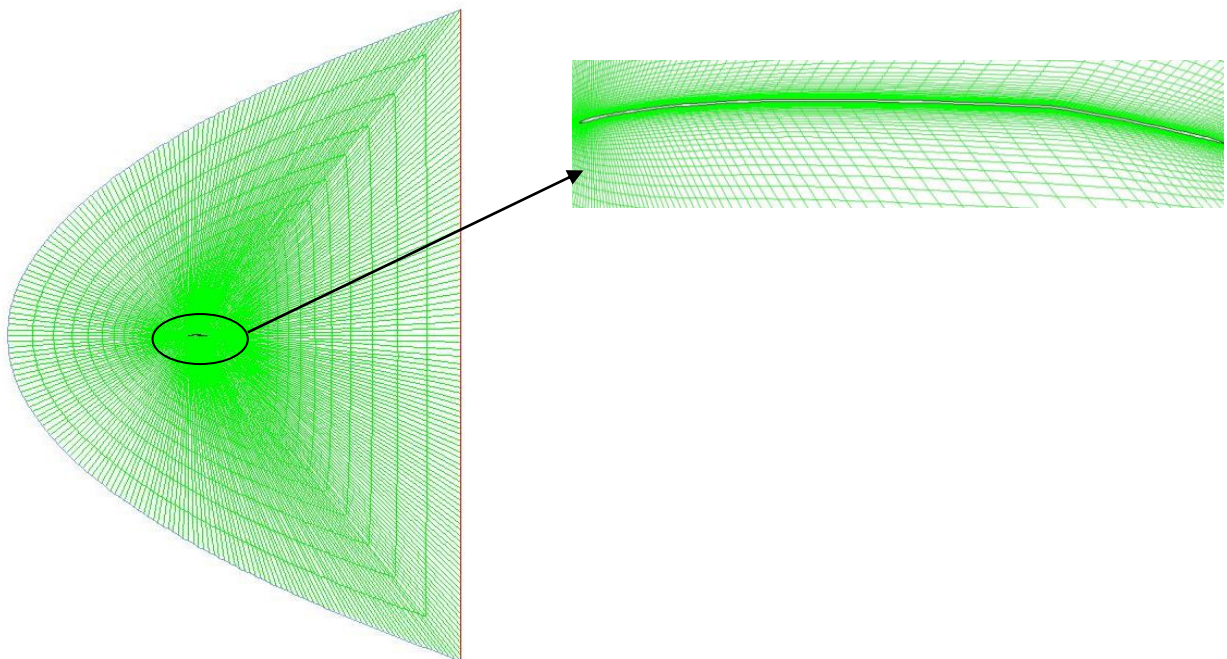


Fig. 15 CFD model used for simulation

The deflected profile (conventional/ morphed) has been modeled using CAD package with C-grid domain. The structured grid model used for CFD simulation is shown in Fig. 15. The grids are carefully generated, surrounding the profile to get the near wall function Y^+ value close to one, in order to accurately predict the viscous affected region.

To capture the effect of boundary layer, the mesh near the wall was carefully determined with approximate first cell distance from the wall as 1.5×10^{-6} m and with a growth factor of 1.16. The multi block structured grid was applied in the modeling of the conventional and morphed camber plates and the mesh consists of approximately 30,000 cells.

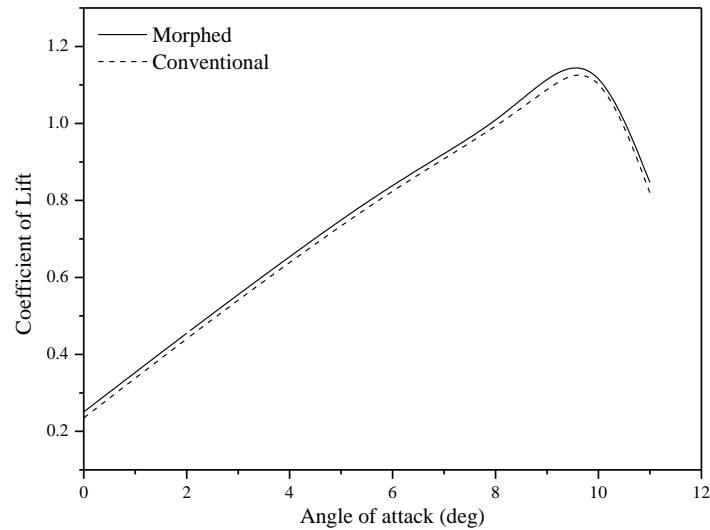


Fig. 16(a) Coefficient of lift Vs Angle of Attack (C_l Vs α) with downward deflection

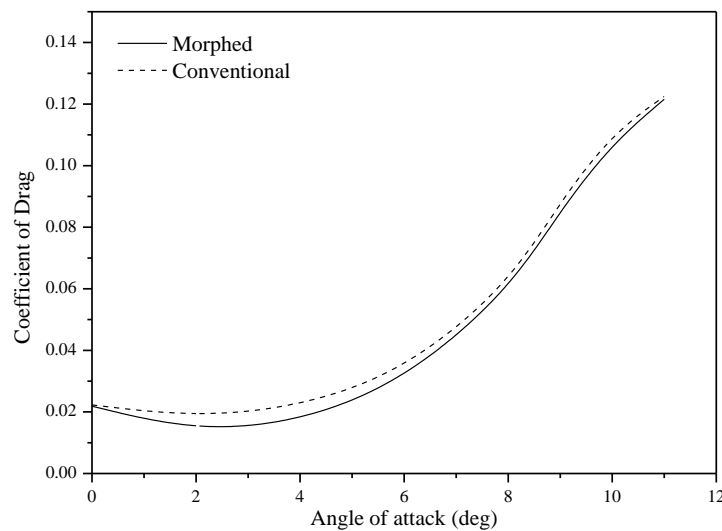


Fig. 16(b) Coefficient of drag Vs Angle of Attack (C_d Vs α) with downward deflection

7.1 Studies on upward deflection of elevon

Through morphing of BK MAV, an upward deflection of 3 mm is achieved, which induces 2.65 deg of upward motion. To get the same control derivatives achieved by morphed MAV, the conventional MAV has to deflect its control surfaces by 3.4 deg. It is observed that the morphed elevon shows a significant improvement in lift coefficient compared to the conventional elevon with $C_{l_{max}}$ increment of over 3.3 % (see Fig. 16(a)). $C_{l_{max}}$ improvement shows that MAV's stall speed may be reduced, i.e. the MAV can be hand launched with lower velocity that is good for BK MAV.

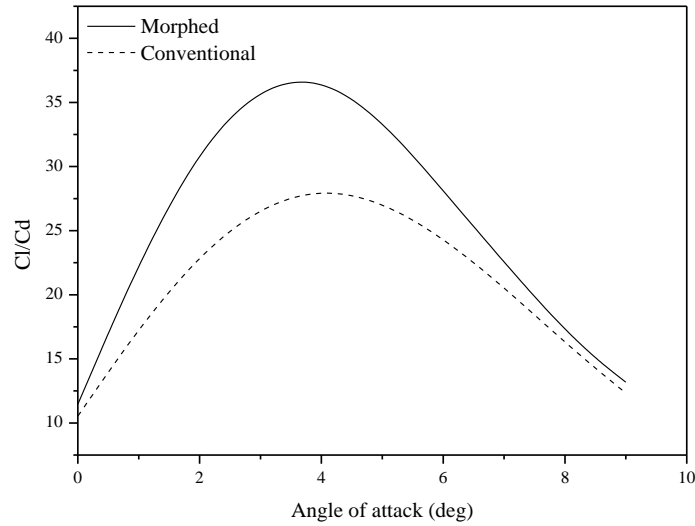


Fig. 16(c) Aerodynamic characteristics of elevon with upward deflection (C_l/C_d Vs α)

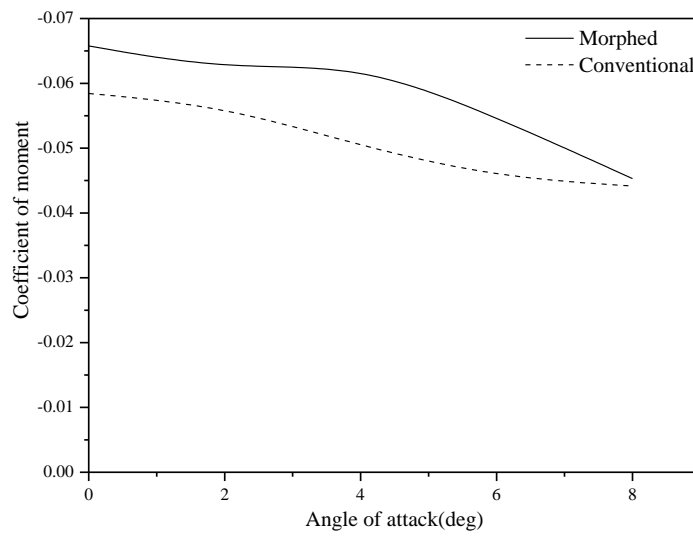


Fig. 16(d) Coefficient of moment Vs Angle of Attack with upward deflection

An average of 12% decrement in drag was observed as in Fig. 16(b) for the morphed elevon case over the conventional one; therefore the performance of the MAV with morphed wing during cruise and loiter phase will significantly improve. The drag produced by conventional elevon is higher than morphed elevon, since it may be expected for a discontinuous trailing edge geometry that will be prone to viscous effects. As the angle of attack increases the difference in drag between the two configurations decreases due to separation effects since the cambered plate will be nearing the stall condition. It is further seen that the continuous (morphed) trailing edge through morphing is aerodynamically streamlined than the conventional control surface in deployed position.

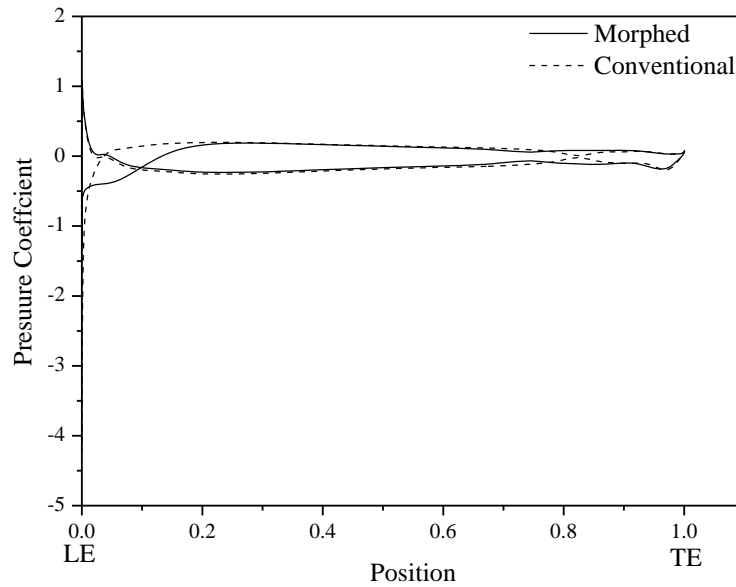


Fig. 17(a) Pressure distribution at AOA = 0 deg

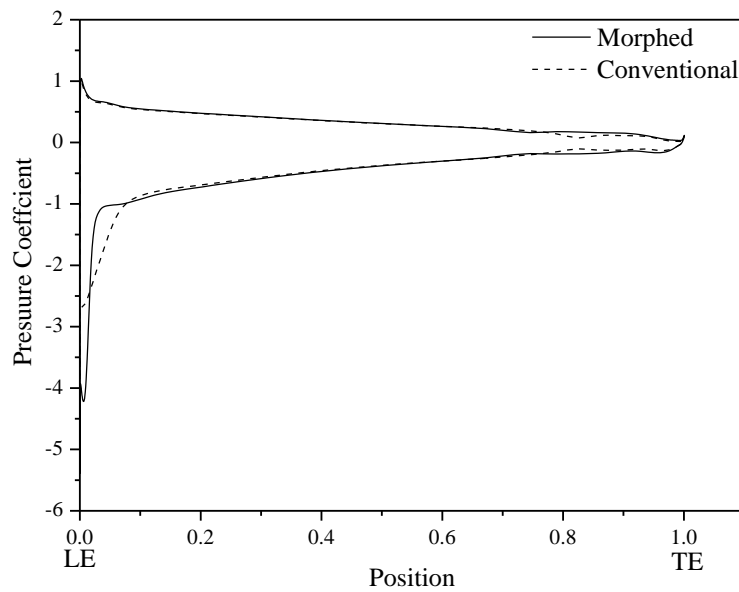


Fig. 17(b) Pressure distribution at AOA = 6 deg

The maximum improvement of 25% in C_l/C_d ratio is observed at 4 deg (refer to Fig. 16(c)). During the operation of BK MAV, most of the time, the control surface will be deflected upward; therefore improvement in aerodynamic efficiency can improve the range and endurance of the vehicle. The pitching moment coefficient is computed at quarter chord of the cambered plate. From the Fig. 16(d), the moment coefficient is seen highly negative for morphed elevon, hence tends to produce more pitching moment during the MAV operation.

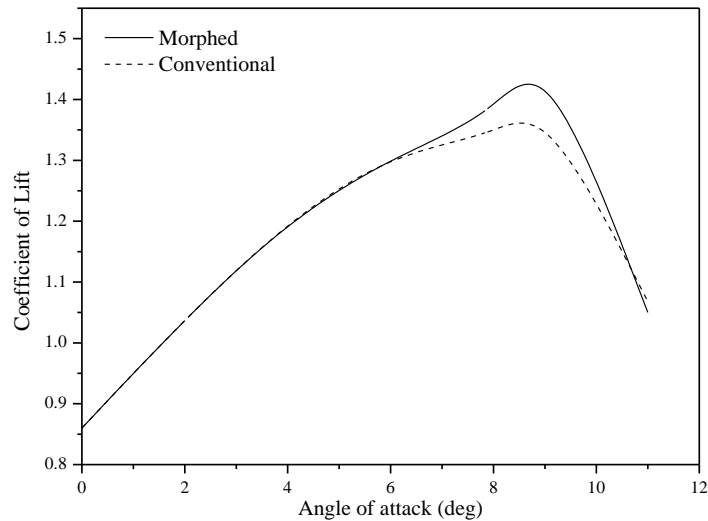


Fig. 18(a) Coefficient of lift Vs Angle of Attack (C_L Vs α) with downward deflection

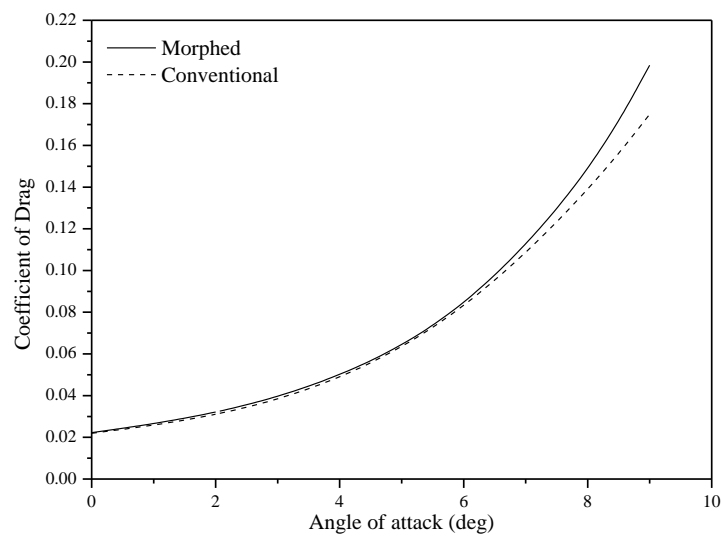


Fig. 18(b) Coefficient of drag Vs Angle of Attack (C_D Vs α) with downward deflection

From Fig. 17(a), (b), it can be observed that a small change in the trailing edge geometry can influence much the upstream flow characteristics. In addition, the hinge axis can be identified clearly in the conventional elevon due to significant change in the pressure coefficient slope, but in the morphed elevon case, this radical change in slope was not observed due to smooth contour variation of the profile.

7.2 Studies on downward deflection of elevon

In the downward morphing, 7.8 mm deflection is achieved, which induces 7 deg motion.

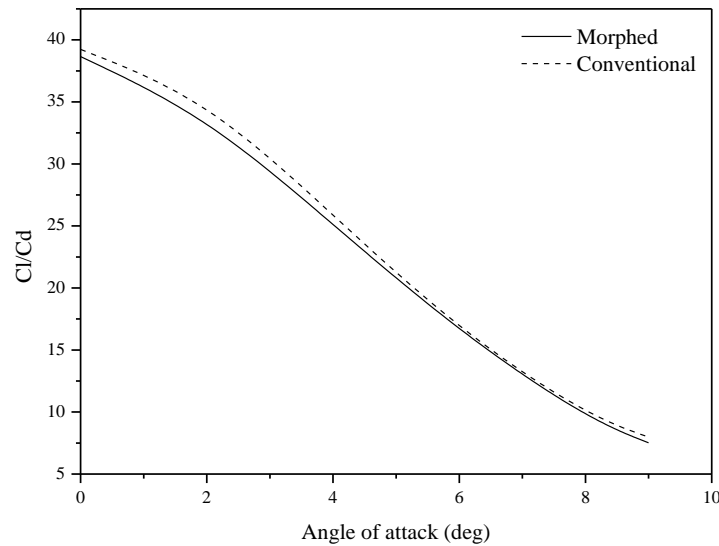


Fig. 18(c) Aerodynamic characteristics of elevon with downward deflection (C_l/C_d Vs α)

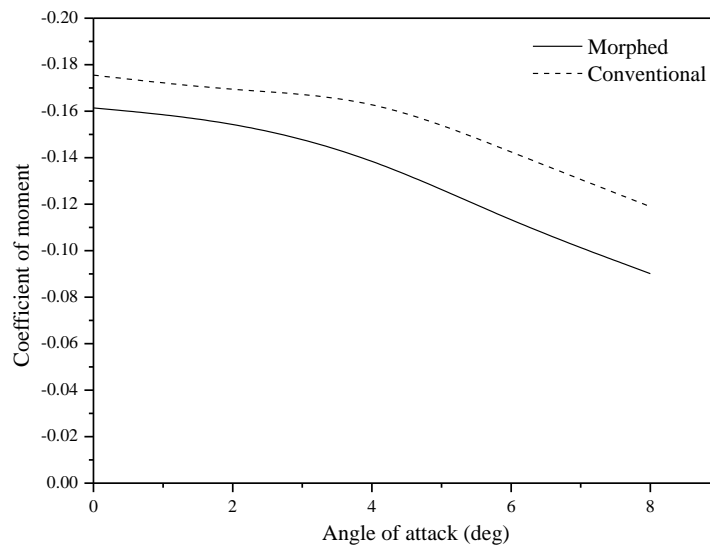


Fig. 18(d) Coefficient of moment Vs Angle of Attack with downward deflection

However, the conventional BK MAV has to deflect its control surface by 8.7 deg to have same aerodynamic performance. From the Fig. 18(a), the lift is almost same at lower angles of attack for the conventional and morphed elevon but C_{lmax} increment of over 6.4% is observed for the morphed elevon at higher angles of attack.

BK MAV has been designed for belly landing and its most aft portion of the fuselage will have to hit the ground first. It is therefore required that aerodynamically the vehicle needs to develop higher drag (refer Fig. 18(b)) during landing at high angle of attack. This may be achieved through trailing edge morphing, so the landing distance and the touchdown speed of BK MAV can be

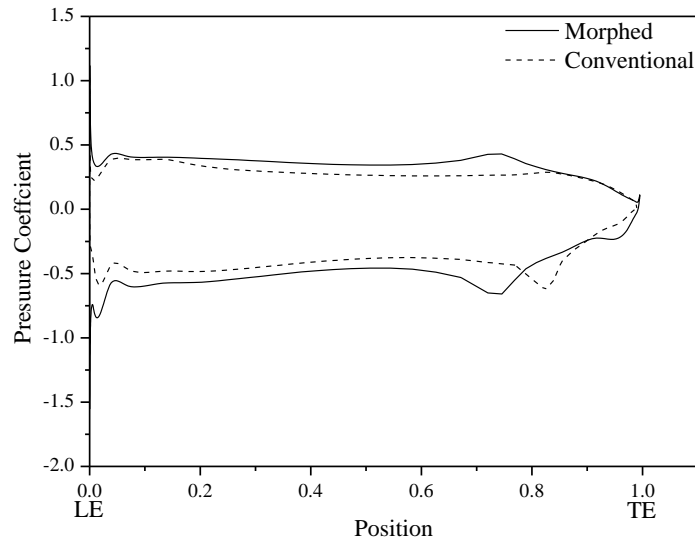


Fig. 19(a) Pressure distribution at AOA = 0 deg

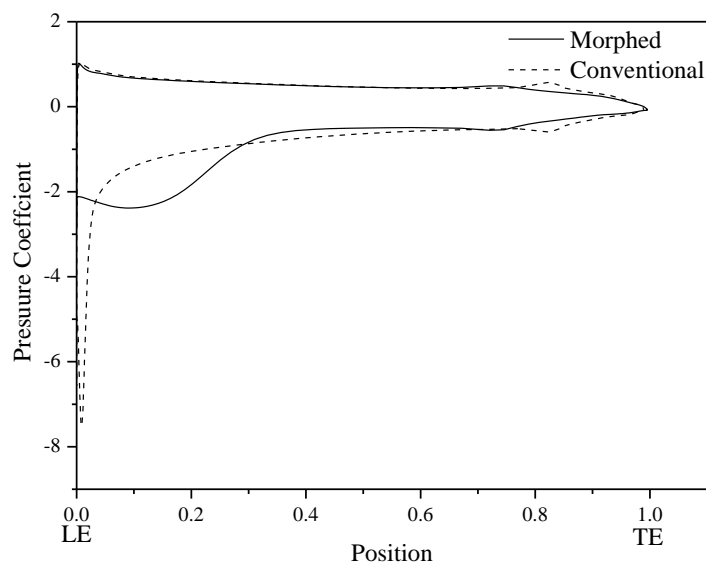


Fig. 19(b) Pressure distribution at AOA = 6 deg

reduced significantly (see in Fig. 18(c)).

It is evident from the Fig. 18(d), that the pitching moment coefficient of the conventional elevon is higher than the morphed case. Remember that for a stable BK MAV flight, the elevons need to be deflected upward during cruise and loitering. From the Fig. 19(a) and 19(b), an increase in pressure difference is noticed for the morphed elevon, which is the basis for the lift increment. In addition, a gradual increment of pressure and velocity is observed near the hinge axis in morphed case over conventional elevon. This leads to uniform load distribution near the hinge axis rather than concentrated loading.

8. Conclusions

A trailing edge wing surface morphing concept is developed and demonstrated using piezoelectric composite actuators, commercially known as MFC. Numerical modeling and experimental validation is done accordingly. Further, through static aeroelastic analysis, it has been shown that the morphed trailing wing surface can be deployed in the elevator and aileron modes for achieving aerodynamic trim conditions. The aerodynamic improvement of 7% aileron reversal speed is achieved, besides an enhanced effectiveness of the morphed elevons over conventional one. Moreover an increment of 38% in turn rate and turn radius is achieved during roll maneuver. The aerodynamics of morphed cambered plate have shown better efficiency (C_l/C_d) for different modes of operation of BK MAV over conventional elevons.

Acknowledgements

The authors wishes to thank Mr. M P Vijayakumar, Mrs. V Sudha, Miss A Sharmila, Mr. Jayanthulu, Mr. S Vedhaprakash, Mr. M Srinivas for their technical contributions/discussions and support during the experimental and analytical works.

References

- Barbarino, S., Bilgen, O., Ajaj, R.M., Friswell, M.I. and Inman, D.J. (2011), "A review of morphing aircraft", *J. Intel. Mater. Syst. Struct.*, **22**(9), 823-877.
- Barbarino, S., Saavedra Flores, E.L., Ajaj, R.M., Dayyani, I. and Friswell, M.I. (2014), "A review on shape memory alloys with applications to morphing aircraft", *Smart Mater. Struct.*, **23**(6), 063001..
- Bilgen, O., Butt, L.M., Day, S.R., Sossi, C.A., Weaver, J.P., Wolek, A., Mason, W.H. and Inman, D.J. (2013), "A novel unmanned aircraft with solid-state control surfaces: analysis and flight demonstration", *J. Intel. Mater. Syst. Struct.*, **24**(2), 147-167.
- Bilgen, O. and Friswell, M.I. (2014), "Piezoceramic composite actuators for a solid-state variable-camber wing", *J. Intel. Mater. Syst. Struct.*, **25**(7), 806-817.
- Bilgen, O., Kochersberger, K., Diggs, E.C., Kurdila, A.J. and Inman, D.J. (2007), "Morphing wing micro-air-vehicles via macro-fiber-composite actuators", *AIAA 2007-1785, 48thAIAA/ASME/ASCE/AHS/ASC Structures, Structural Dynamics, and Materials Conference*, Honolulu, Hawaii, April.
- Bilgen, O., Kochersberger, K.B., Inman, D.J. and Ohanian, O.J. (2010), "Lightweight High Voltage Electronic Circuits for Piezoelectric Composite Actuators", *J. Intel. Mater. Syst. Struct.*, **21**(14), 1417-1426.
- Bisplinghoff, R.L., Ashley, H. and Halfman, R.L. (2013), *Aeroelasticity*, Courier Dover Publications
- Bradley, L. and Peter, I. (2012), "Finite Element Modeling of Macro Fiber Composite Piezoelectric Actuators on Micro Air Vehicles", *AIAA2012-1903, 53rdAIAA/ASME/ASCE/AHS/ASC Structures, Structural Dynamics and Materials Conference*, Honolulu, Hawaii, April.
- Bradley, W.L. and Peter, I. (2013), "A Study of Substrate Materials for Use in Conjunction with Macro Fiber Composites", *AIAA2013-1916, 54thAIAA/ASME/ASCE/AHS/ASC Structures, Structural Dynamics, and Materials Conference*, Boston, Massachusetts, USA, April.
- Cote, F., Masson, P., Mrad, N. and Cotoni, V. (2004), "Dynamic and static modelling of piezoelectric composite structures using a thermal analogy with MSC/NASTRAN", *Compos. Struct.*, **65**(3-4), 471-484.
- Deraemaeker, A., Nasser, H., Benjeddou, A. and Preumont, A. (2009), "Mixing rules for the piezoelectric properties of macro fiber composites", *J. Intel. Mater. Syst. Struct.*, **20**(12), 1475-1482.

- Gomez, J.C. and Garcia, E. (2011), "Morphing unmanned aerial vehicles", *Smart Mater. Struct.*, **20**(10), 103001..
- Kuder, I.K., Arrieta, A.F., Raither, W.E. and Ermanni, P. (2013), "Variable stiffness material and structural concepts for morphing applications", *Prog. Aerospace Sci.*, **63**, 33-55.
- LaCroix, B.W. and Ifju, P.G. (2012), "Utilization and performance enhancements of multiple piezoelectric actuators on micro air vehicles", *AIAA 2012-0392, 50th AIAA Aerospace Sciences Meeting including the New Horizons Forum and Aerospace Exposition*, Nashville, Tennessee, USA, January.
- MSC Nastran (2012), "Linear Static Analysis User's Guide", MSC Software Inc, USA.
- Ohanian, O.J., Hickling, C., Stiltner, B., Karni, E.D., Kochersberger, K.B., Probst, T., Gelhausen, P.A. and Blain, A.P. (2012), "Piezoelectric morphing versus servo-actuated MAV control surfaces", *AIAA 2012-1512, 53rd AIAA/ASME/ASCE/AHS/ASC Structures, Structural Dynamics and Materials Conference*, Honolulu, Hawaii, April.
- Osgar, O., Brian, D., Seth, T., Kevin, K., Troy, P., Paul, G. and Jonathon, C. (2013), "Piezoelectric morphing versus servo-actuated MAV control surfaces, Part II: flight testing", *AIAA 2013-0767, 51st AIAA Aerospace Sciences Meeting including the New Horizons Forum and Aerospace Exposition*, Grapevine (Dallas/Ft. Worth Region), Texas, USA, January.
- Pankonien, A. and Inman, D.J. (2013), "Experimental testing of spanwise morphing trailing edge concept", *Proc. SPIE 8688, 868815, April 10, 2013, Active and Passive Smart Structures and Integrated Systems 2013*, San Diego, California, USA.
- Paradies, R. and Ciresa, P. (2009), "Active wing design with integrated flight control using piezoelectric macro fiber composites", *Smart Mater. Struct.*, **18**(3), 035010.
- Pelletier, A. and Mueller, T.J. (2000), "Low Reynolds number aerodynamics of low-aspect-ratio, thin/flat/cambered-plate wings", *J. Aircraft.*, **37**(5), 825-832.
- Probst, T.A., Kochersberger, K., Stiltner, B., Hickling, C.J., Ohanian Iii, O.J., Karni, E., Olien, C. and Blain, A.P. (2012), "Smart material actuators as a means of UAV flight control", *AIAA 2012-0486, 50th AIAA Aerospace Sciences Meeting including the New Horizons Forum and Aerospace Exposition*, Nashville, Tennessee, USA, January.
- Rodden, W.P. and Johnson, E.H. (1994), *MSC/NASTRAN aeroelastic analysis: user's guide; Version 68*, MacNeal-Schwendler Corporation.
- Roshan Antony, Suraj, C.S. and Sankara Narayanan, S. (2011), *Design of Black Kite Micro Air Vehicle*, PD PR 1121, CSIR-National Aerospace Laboratories, Bangalore.
- Sadraey, M.H. (2012), *Aircraft Design: A Systems Engineering Approach*, John Wiley & Sons.
- Sanders, B., Eastep, F.E. and Forster, E. (2003), "Aerodynamic and Aeroelastic Characteristics of Wings with Conformal Control Surfaces for Morphing Aircraft", *J. Aircraft.*, **40**(1), 94-99.
- Sofla, A.Y.N., Meguid, S.A., Tan, K.T. and Yeo, W.K. (2010), "Shape morphing of aircraft wing: Status and challenges", *Mater. Des.*, **31**(3), 1284-1292.
- Vale, J., Leite, A., Lau, F. and Suleman, A. (2011), "Aero-structural optimization and performance evaluation of a morphing wing with variable span and camber", *J. Intel. Mater. Syst. Struct.*, **22**(10), 1057-1073.
- Weisshaar, T.A. (2013), "Morphing aircraft systems: historical perspectives and future challenges", *J. Aircraft.*, **50**(2), 337-353.
- Wickramasinghe, V., Chen, Y., Martinez, M., Wong, F. and Kernaghan, R. (2011), "Design and verification of a smart wing for an extreme-agility micro-air-vehicle", *Smart Mater. Struct.*, **20**(12), 125007.
- ANSYS Fluent Theory Guide (2011), Release 14.0, ANSYS Inc, Southpointe, Canonsburg, PA, 15317, November.
- Macro Fiber Composite - MFC, Smart Material Corp., www.smart-material.com.

Nomenclature

GFRP	Glass Fibre Reinforced Plastics
AR	Aspect Ratio
$\{\sigma\}$	Stress Vector (6×1) (N/m ²)
$\{\varepsilon\}$	Strain Vector (6×1)
$\{E\}$	Electric Field Vector (3×1) (V/m)
$[C^E]$	Elastic Stiffness co-efficient matrix (6×6) (N/m ²)
$[d]$	Piezoelectric Coupling matrix (3×6) (C/N or m/V)
$\{\alpha\}$	Thermal Expansion co-efficient vector (6×1) (1/°C)
ΔT	Temperature difference (°C)
T_0	Reference Temperature (°C)
h_a	Electric field thickness between the electrodes (m)
α_i	Thermal expansion coefficient per each direction (i) (1/°C)
A_m	Area of morphed control surface
A_c	Area of conventional control surface
δ_a	Anti-symmetric elevon deflection
$C_{L\delta e}$	Slope of lift coefficient due to elevon deflection
$C_{M\delta e}$	Slope of pitching moment coefficient due to elevon deflection
$C_{L\delta a}$	Slope of rolling moment coefficient due to elevon deflection
C_{Lp}	Roll damping
$\frac{pb}{2V}$	Roll helix angle induced by rolling motion
LE	Leading Edge
TE	Trailing Edge